

Effect of Prior Recovery Treatment on the Evolution of Cube Texture During Annealing of Severely Warm-Rolled Al-2.5 wt pctMg Alloy



J.R. GATTI and PINAKI PRASAD BHATTACHARJEE

The effect of prior recovery on the evolution of cube texture ($\{001\}\langle 100\rangle$) in severely warm-rolled and annealed Al-2.5 wt pctMg alloy was studied. The Al-2.5 wt pctMg alloy was warm rolled to 97 pct reduction in thickness at 473 K (200 °C). The warm-rolled sheets were isochronally annealed for 1 hour at temperatures ranging from 523 K to 673 K (250 °C to 400 °C) without and with prior recovery treatments. In case of prior recovery, the sheets were pre-treated at 473 K (200 °C) for different time intervals ranging from 3.6×10^3 seconds (1 hour) to 8.64×10^4 seconds (24 hours) before the annealing. The warm-rolled alloy showed finely subdivided lamellar structure and strong presence of pure metal type texture. The annealed materials without any prior recovery treatment showed strong cube texture after annealing which could be attributed to the oriented nucleation of cube grains resulting from the preferentially recovered structure of cube regions in the warm-rolled state. In contrast, the cube texture was significantly weakened in materials subjected to different prior recovery treatments. The prior recovery treatments resulted in homogenous recovery which was confirmed by microstructural, textural, and conductivity measurements. Homogenous recovery eliminated the nucleation advantage of cube regions originating from the preferentially recovered structure and weakened the cube texture significantly. The present results indicated that prior recovery treatment could be effectively used to control recrystallization cube texture in severely warm-rolled aluminum alloys.

DOI: 10.1007/s11661-015-3129-4

© The Minerals, Metals & Materials Society and ASM International 2015

I. INTRODUCTION

THERMO-MECHANICAL processing of materials leads to the development of prominent crystallographic textures in different metals and alloys. The development of sharp crystallographic texture can greatly affect the anisotropic mechanical behavior. As a result, extensive studies have been carried out on the evolution of microstructure and texture in face-centered cubic (FCC) materials during thermo-mechanical processing.^[1,2] It has been clarified that stacking fault energy (SFE) of materials greatly affects the evolution of deformation texture, such that high-to-medium SFE materials develop pure metal or copper-type texture characterized by strong Cu ($\{112\}\langle 111\rangle$), S ($\{123\}\langle 634\rangle$), and brass or B_S ($\{110\}\langle 112\rangle$) components, whereas in low SFE materials, brass type texture dominated by the B_S component is observed.^[3]

The process of annealing following heavy deformation in medium-to-high SFE materials frequently results in the formation of strong cube texture ($\{001\}\langle 100\rangle$) although the cube has a negligible presence in the

deformed structure. It might be pointed out that the annealing texture of heavily deformed aluminum alloys may be quite complex, often revealing the presence of cube ($\{001\}\langle 100\rangle$), ND-rotated cube (or Q) ($\{013\}\langle 231\rangle$),^[4,5] R ($\{124\}\langle 211\rangle$) originating from the deformation texture component (S),^[6-9] and $\{011\}\langle 455\rangle$ (or P) orientations.^[10-13] The different annealing texture may be obtained in the same aluminum alloy by varying homogenization and annealing conditions.^[14]

The origin of the cube texture has been explained on the basis of oriented nucleation (ON) or oriented growth (OG).^[15] In the ON theory, development of strong cube texture is attributed to preferential nucleation of cube grains from the thin cube-oriented regions pre-existing in the deformed matrix in the transition bands^[16] or as fragments (cube bands) of the original cube-oriented grains.^[17] Careful experimental studies^[17-20] have revealed orientation dependent preferential recovery in cube-oriented regions due to the unique dislocation interaction involving orthogonal burgers vectors.^[21] In contrast, in the OG model, the origin of the sharp cube texture is explained on the basis of preferential growth of cube grains due to the favorable high-mobility misorientation relationship between the cube grains and surrounding deformed matrix.

The control of cube texture is particularly important for achieving enhanced formability in aluminum alloys for different applications. As a result, the control of the cube texture remains a topic of much interest during

J.R. GATTI, PhD Student, and PINAKI PRASAD BHATTACHARJEE, Associate Professor, are with the Department of Materials Science and Metallurgical Engineering, Indian Institute of Technology Hyderabad, Yeddumailaram, Telangana 502205, India. Contact email: pinakib@iith.ac.in

Manuscript submitted October 5, 2014.

Article published online September 8, 2015

thermo-mechanical processing of aluminum alloys. In precipitation strengthened alloys, the deformation zones around the sufficiently large second-phase particles can result in particle-stimulated nucleation (PSN) weakening the strength of the recrystallization cube texture.^[22] In addition, the annealing texture of aluminum alloys can also be significantly influenced and controlled by microchemistry and precipitation states,^[23] temperature,^[24] strain path,^[25] and prior recovery.^[26]

Among different parameters, the effect of prior recovery has been studied only to a limited extent. It has been reported that prior recovery treatment can weaken the strength of recrystallization cube texture in heavily cold-rolled Al-Mg alloy although the detailed mechanism of this has not been reported.^[26] However, from the point of view of controlling recrystallization texture, this effect evidently remains quite interesting. Recent investigation on heat-treatable cold-rolled aluminum alloys reports that prior recovery annealing can significantly modify the relative strength of the recrystallization texture components.^[27]

In the present work, we investigate the effect of prior recovery treatment over wide time intervals on the evolution of cube texture in severely warm-rolled and annealed Al-2.5 wt pctMg alloy. Thermo-mechanical processing by warm rolling of aluminum alloys has been investigated previously and most of the times with an objective to control texture by the formation of shear texture components.^[28–31] On the other hand, the effect of prior recovery treatment on the evolution of recrystallization texture has been investigated mostly in cold-rolled alloys.^[26,27]

II. EXPERIMENTAL

A. Processing

Al-Mg blocks having dimensions 150 mm (length) \times 60 mm (width) \times 10 mm (thickness) having a chemical composition shown in Table I were obtained from Testbourne Ltd., UK. The as-received blocks were initially cold rolled to \sim 50 pct reduction in thickness using a laboratory scale rolling mill having roll diameter of 140 mm. The cold-rolled materials were subsequently annealed at 673 K (400 °C) for 4 hours. The annealed materials were further cold rolled to \sim 80 pct reduction in thickness to a thickness of \sim 1 mm and annealed at 573 K (300 °C) for 3 hours. The annealed sheets were used as the starting materials for subsequent warm rolling.

The warm-rolling was carried out by a novel combination of accumulative roll bonding (ARB) which is a well-known severe plastic deformation technique for sheet metal processing^[32] and conventional rolling (*i.e.*, typical cold rolling during which the thickness of the sheet continuously decreases with increasing

deformation as opposed to ARB). For this purpose, two sheets of Al-Mg alloy with thickness of 1 mm were subjected to typical ARB processing comprising of surface cleaning (*i.e.*, degreasing with acetone), wire brushing, stacking of the sheets, and roll bonding by imparting \sim 50 pct reduction (equivalent strain (ϵ_{eq}) \sim 0.8) in a single pass. In the next ARB cycle, the roll-bonded sheets were again cut into halves, and the above steps were repeated. In the present work, the ARB process was carried up to three cycles ($\epsilon_{eq} \sim$ 2.4, equivalent to a thickness reduction of \sim 87.5 pct in terms of conventional rolling) during which the sheet thickness was maintained at \sim 1 mm. The ARB processing was followed by conventional rolling to 75 pct reduction in thickness ($\epsilon_{eq} \sim$ 4, equivalent to a total thickness reduction of \sim 97 pct) to a final thickness of \sim 250 μ m. The warm-rolling was carried out at 473 K (200 °C). The sheets were isothermally held at 473 K (200 °C) in a muffle furnace for 600 seconds (10 min) before every warm-rolling pass. The rolls were pre-heated to 473 K (200 °C) to minimize the heat loss during warm rolling. The sheets were quenched in cold water after every warm-rolling pass.

The 97 pct warm-rolled materials were annealed with and without prior recovery treatments. In case of annealing without prior recovery, warm-rolled coupons were isochronally annealed for 1 hour in a salt bath furnace at temperatures ranging from 473 K to 673 K (200 °C to 400 °C). In case of prior recovery treatment, the warm-rolled coupons were first isothermally annealed at 473 K (200 °C) for different annealing times ranging from 1 hour to 24 hours. These pre-recovery-treated samples were further isochronally annealed for 1 hour at 523 K, 548 K, and 673 K (250 °C, 275 °C, and 400 °C). The annealed materials were immediately quenched in cold water following the annealing treatments.

B. Characterization

The microstructures and texture of the materials were investigated using an electron backscatter diffraction (EBSD) system (Oxford Instruments, UK) attached to a scanning electron microscope (SEM) having a field emission gun (FEG) source (Carl-Zeiss, Germany, Model: Supra 40). Samples for EBSD measurement were prepared by careful mechanical polishing followed by electropolishing (electrolyte: 10 pct perchloric acid + 90 pct methanol, temperature: -30 °C, voltage: 20 V). The scan step size for the deformed (*i.e.*, as warm-rolled materials) and partially recrystallized materials was 0.04 μ m (40 nm). For each annealed sample, several EBSD scans having areas varying from 600 \times 600 μ m² to 900 \times 900 μ m² were acquired to obtain statistically reliable texture results. For the annealed samples, the scan step size varied from 1.0 to 1.5 μ m. The fraction of indexed points in case of the different fully annealed samples was more than 85 pct. For the recovery-treated samples, the fraction of indexed points varied from 50 to 70 pct. The acquired EBSD data were exported to the TSL-OIM™ software (EDAX Inc., USA) for analysis purpose. EBSD dataset were cleaned up using the

Table I. Chemical Composition of the As-Received Alloy

Fe	Si	Ca	Cu	Mg	Al
15.0 ppm	5.0 ppm	5.0 ppm	20.0 ppm	2.51 wt pct	bal

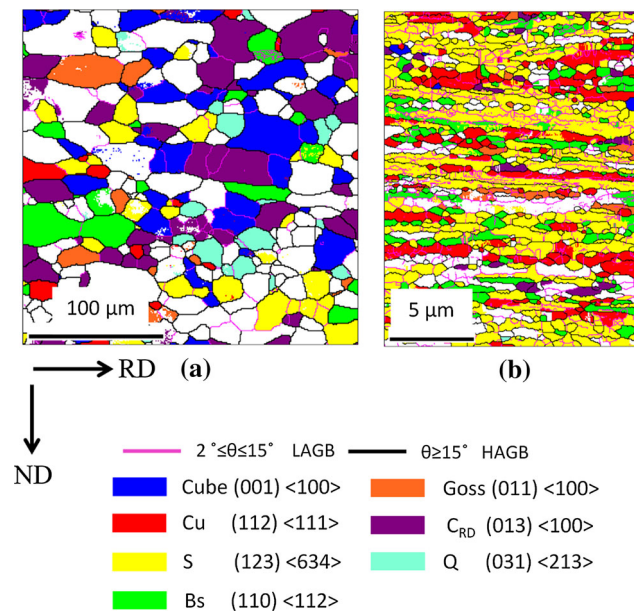


Fig. 1—Orientation maps of the (a) starting recrystallized and (b) 97 pct warm-rolled materials (Color figure online).

standard grain dilation procedure imposing the criteria of grain tolerance angle 5 deg, grain size with minimum five scan points, and multiple scan rows. The pole figures (PFs) and orientation distribution functions (ODFs) were calculated from merged EBSD dataset using the series expansion method with series rank 22. Orientations of at least 3000 recrystallized were considered for calculating the PFs and ODFs. The volume fraction of different texture components was determined using a tolerance angle of 15 deg. In case of an overlap, the orientation which is closest to the indexed point is assigned that orientation.

The electrical conductivity of the different pre-recovery-treated samples was determined by the standard 4-probe method (Keithley, Germany; Model: 2611B). A consistent current value 0.01 A was used for this purpose.

III. RESULTS

Figure 1 shows the microstructure and texture of the starting and heavily warm-rolled materials. Figure 1(a) reveals the fully recrystallized microstructure of the starting material having an average grain size of $\sim 15 \mu\text{m}$. The spatial distribution of different texture components is also shown in Figure 1(a) which also confirms the strong presence of cube (highlighted in blue) and RD-rotated cube component (C_{RD} ; $\{013\}\langle 100 \rangle$; highlighted in purple). The orientation map also reveals only minor presence of the ND-rotated cube component (Q; $\{031\}\langle 213 \rangle$; highlighted in cyan) as compared to S ($\{123\}\langle 634 \rangle$, highlighted in yellow), B_S ($\{110\}\langle 112 \rangle$, highlighted in green), copper (or Cu) ($\{111\}\langle 112 \rangle$, highlighted in red), and Goss (or G) ($\{011\}\langle 100 \rangle$, highlighted in orange). The ODF sections

of the starting material (Figure 2(a)) calculated from the merged dataset also confirm the presence of strong cube and C_{RD} components.

The orientation map of the 97 pct warm-rolled material (Figure 1(b)) shows the development of an ultrafine lamellar microstructure extended parallel to the RD. The orientation map shows profuse Cu-, S-, and R-oriented grains but negligible presence of the cube orientation. The $\varphi_2 = 0 \text{ deg}$, 45 deg , and 65 deg sections of the ODF of 97 pct warm-rolled are shown in Figure 2(b). The relevant ODF sections suggest significant strengthening of the S and Cu components. This is also clearly understood from Figure 2(c) which summarizes the textural changes quantitatively. The development of stronger S and Cu components as compared to the B_S component may easily be noticed. The development of a pure metal (or copper type) texture after severe warm-rolling is thus quite evident.

Figure 3 shows the microstructures of the warm-rolled material after different pre-recovery treatments. The large area raw (*i.e.* as acquired) inverse pole figure (IPF) maps with respect to the ND after pre-recovery treatment at 473 K (200 °C) for 3.6×10^3 seconds (1 hour) (Figure 3(a)), 21.6×10^3 seconds (6 hours) (Figure 3(b)), and 86.4×10^3 seconds (24 hours) (Figure 3(c)) are shown. Figures 3(d) through (f) show the corresponding IQ maps with overlaid grain boundaries cropped from the original IPF maps and subjected to suitable data clean-up procedure. The microstructures reveal the clear presence of low-angle grain boundary (LAGB) network (highlighted in magenta) and absence of any visible recrystallized regions. The HAGB fractions after annealing for 3.6×10^3 seconds (1 hour), 21.6×10^3 seconds (6 hours), and 86.4×10^3 seconds (24 hours) are found to be ~ 64 , 59, and 58 pct, respectively. It might be noted that similar microstructural evolution and coarsening during prolonged recovery have been extensively investigated in different severely deformed aluminum alloys based on the motion of triple junctions as a possible mechanism.^[33,34]

The $\varphi_2 = 0 \text{ deg}$, 45 deg , and 65 deg sections of the ODFs of different pre-recovered samples are shown in Figure 4. The ODF sections of different pre-recovery-treated materials clearly reveal the strong presence of the deformation texture components. In order to further corroborate the microstructural and textural observations, the electrical conductivities of different pre-recovery-treated samples are shown in Table II. The electrical conductivity of the starting recrystallized material ($24 \times 10^4 \text{ Siemens cm}^{-1}$) is very similar to the value reported elsewhere.^[35] The electrical conductivity shows drastic decrease after severe warm rolling ($3.67 \times 10^4 \text{ Siemens cm}^{-1}$) as compared to that of the starting fully recrystallized material. The electrical conductivity is, however, dramatically increased after different pre-recovery treatments.

In order to understand the effect of prior recovery on the evolution of recrystallization texture, the pre-recovered materials are subsequently annealed for 1 hour at 548 K and 673 K (275 °C and 400 °C). Figure 5 shows the orientation maps of 97 pct warm-rolled and

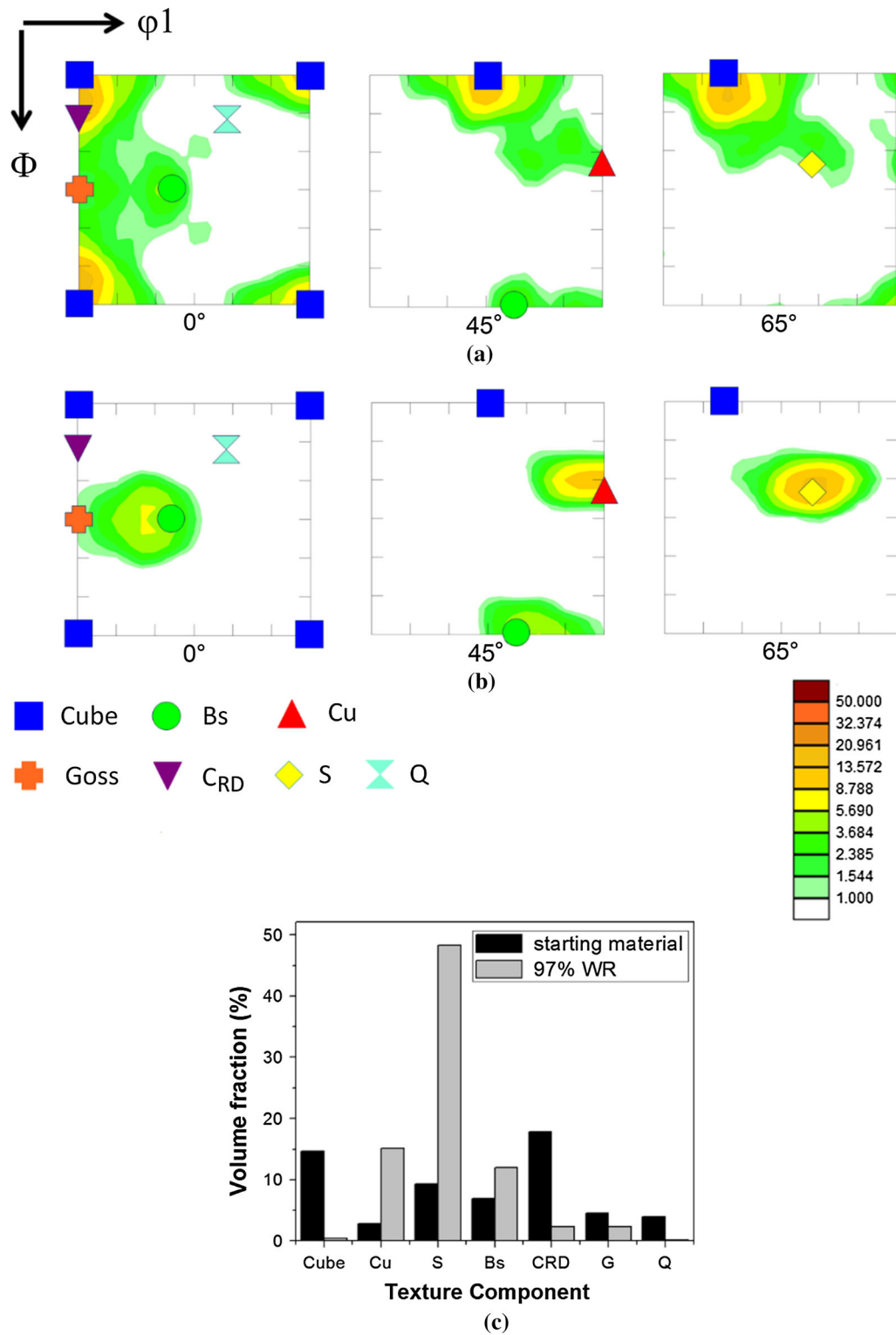


Fig. 2—The relevant ODF sections of (a) starting recrystallized and (b) 97 pct warm-rolled materials; (c) the volume fractions of different texture components in starting and 97 pct warm-rolled Al-2.5 pctMg alloy.

annealed materials with and without prior recovery treatments. The material without any pre-recovery treatment (Figure 5(a)) shows a fully recrystallized microstructure after annealing at 548 K (275 °C). The cube component is remarkably strengthened having an

average volume fraction ~65 pct. The volume fraction of the cube component is increased further (~72 pct) after annealing at 673 K (400 °C) (Figure 5(b)). The strong presence of cube texture is amply corroborated from the $\phi_2 = 0$ deg section of the ODFs of the

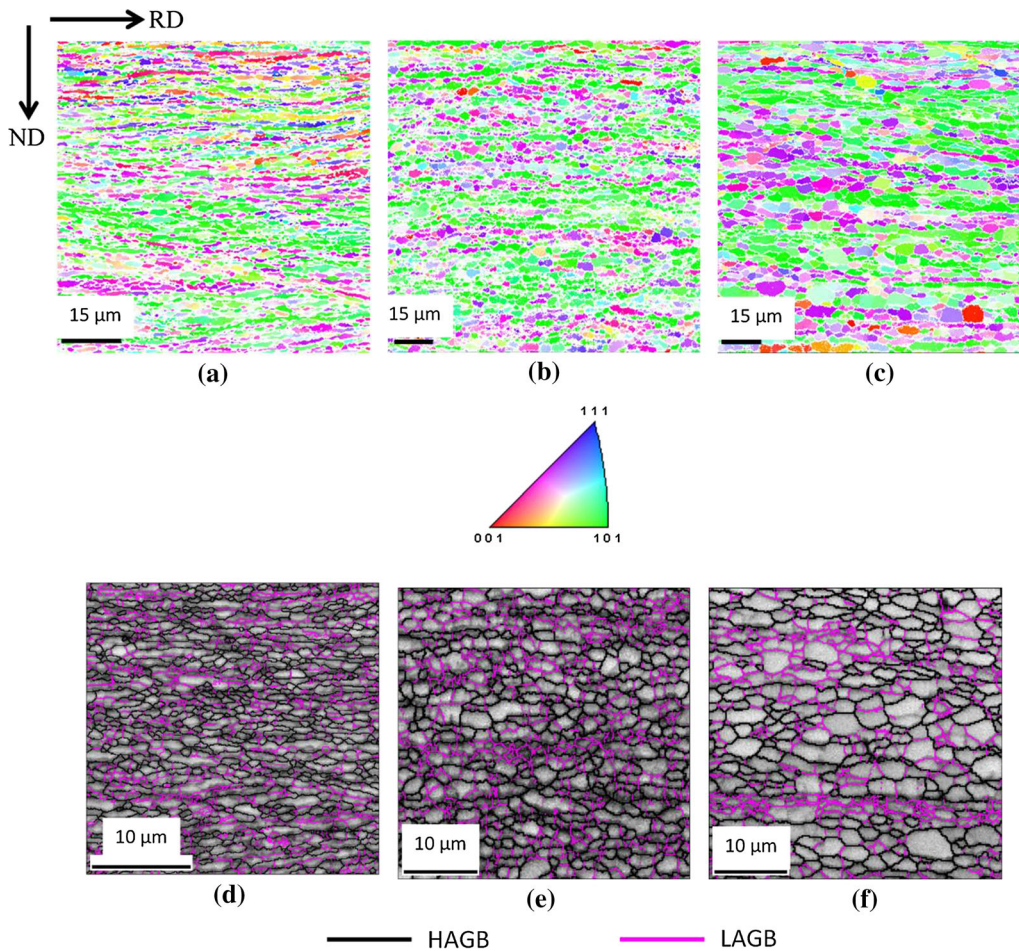


Fig. 3—ND-IPF maps of the 97 pct warm-rolled Al-2.5 wt pctMg alloy recovery treated at 473 K (200 °C) for (a) 3.6×10^3 s (1 h), (b) 21.6×10^3 s (6 h), and (c) 86.4×10^3 s (24 h) (the white dots are unindexed points); (d) to (f) shows the corresponding IQ maps cropped from IPF maps and subjected to suitable data clean-up.

materials annealed at 548 K (275 °C) (Figure 6(a)) and 673 K (400 °C) (Figure 6(b)). Other components are present only in minor proportions which is quite evident from the $\varphi_2 = 0$ deg and 65 deg sections of the ODFs (the $\varphi_2 = 45$ deg section is not shown as copper texture is rather weak in the recrystallization texture) and the orientation maps. In sharp contrast, the material pre-recovery treated at 473 K (200 °C) for 3.6×10^3 seconds (1 hour) shows fully recrystallized microstructure, but a remarkably lower volume fraction of the cube component (~30 pct) after annealing at 548 K (275 °C) (Figure 5(c)). This is also clearly understood from the $\varphi_2 = 0$ deg section of the ODF shown in Figure 6(c). The orientation map (Figure 5(c)) and the $\varphi_2 = 65$ deg section of the ODF (Figure 6(c)) also reveal strong retention of deformation texture-related component, namely R (tan) which has been extensively reported in other aluminum alloys.^[6,8,9,36] The cube volume fraction is increased after annealing at 673 K (400 °C) (Figure 5(d)), yet found to be significantly lower (~47 pct) than the material annealed at the same temperature without any prior recovery treatment (~72 pct).

The orientation maps of the material recovery treated for 21.6×10^3 seconds (6 hours) (Figures 5(e) and (f)) and 86.4×10^3 seconds (24 hours) (Figures 5(g) and (h)) consistently show significantly lower cube volume fraction after different annealing treatments as compared to the material annealed without any prior recovery treatment (Figures 5(a) and (b)). This is also understood by comparing the intensity distribution around the cube location in the relevant ODF sections of these materials (Figures 6(e) through (h)) with that of the material annealed without any pre-recovery treatment (Figures 6(a) and (b)).

The evolution of major recrystallization texture components, namely cube, C_{RD} , and R in materials annealed at 548 K (275 °C) (Figure 5(a)) and 673 K (400 °C) (Figure 5(b)) with and without prior recovery treatments is summarized quantitatively in Figure 7. It is clearly observed that prior recovery treatment reduces the strength of the cube texture, but increases the fraction of the R component. The strength of the cube texture is increased with increasing annealing temperatures (compare Figures 5(a) and (b)) in material without and with prior recovery treatments. The cube and C_{RD} components are strengthened after annealing at 548 K

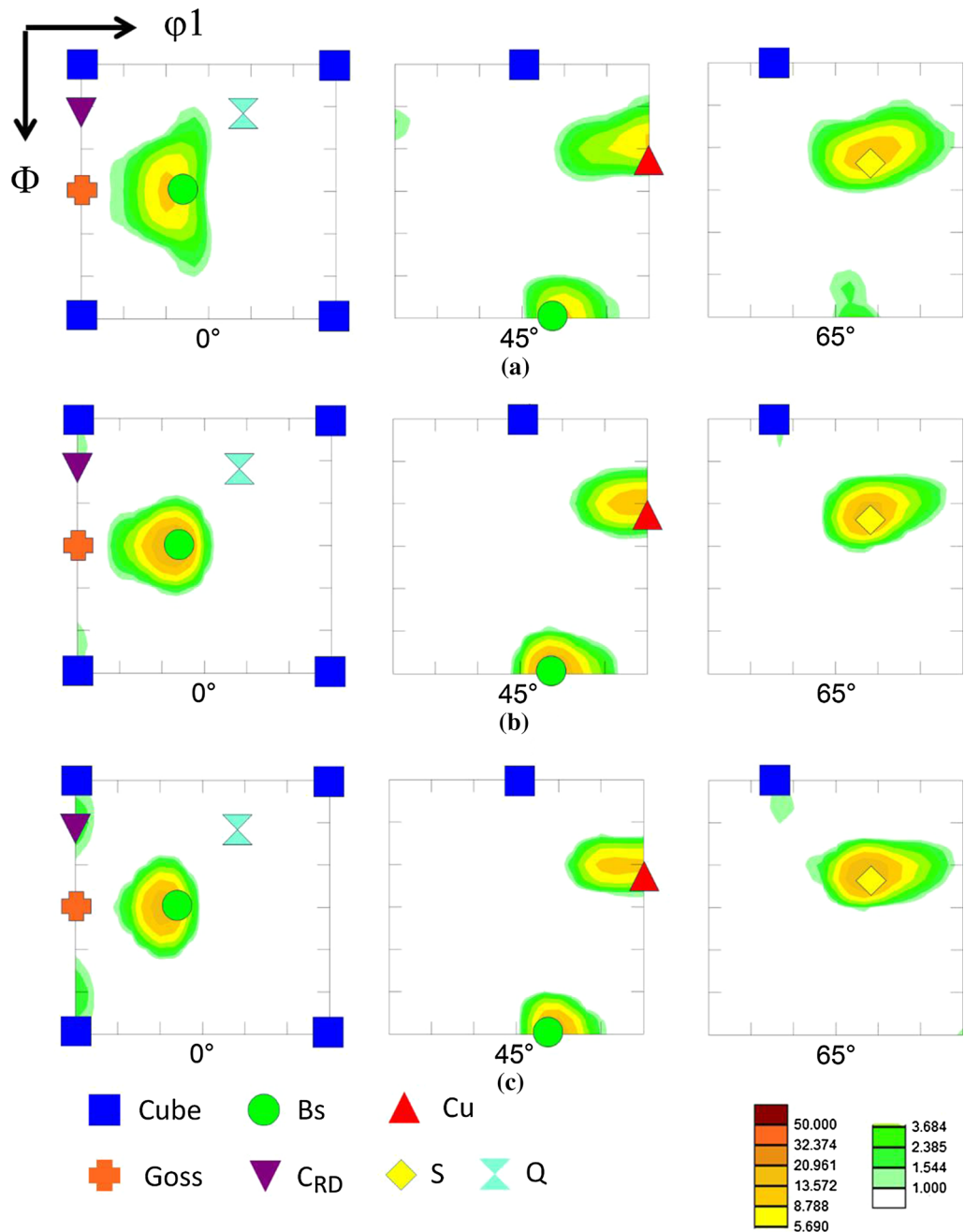


Fig. 4—The $\phi_2 = 0$ deg, 45 deg, and 65 deg sections of the ODFs of 97 pct warm-rolled Al-2.5 wt pctMg alloy recovery treated at 473 K (200 °C) for (a) 3.6×10^3 s (1 h), (b) 21.6×10^3 s (6 h), and (c) 86.4×10^3 s (24 h).

(275 °C) in material prior recovery treated for 24 hours as compared to those in the material prior recovery treated for 6 hours. However, the individual volume fraction of C and C_{RD} and the sum of these components remain substantially lower than the material annealed without prior recovery. It may be further noticed that the cube volume fraction is lower in the material recovery treated for 6 hours as compared to the material recovery treated for 24 hours after annealing at 673 K (400 °C), although the total volume fraction of the cube and C_{RD} remains unchanged (~60 pct).

Table II. Electrical Conductivities of the 97 pct Warm-Rolled and Prior Recovery-Treated Materials

Heat-Treated Condition	Conductivity ($\times 10^4$) Siemens/cm
Starting fully recrystallized material	24.0
97 pct warm rolled	3.67
Recovery treated at 473 K (200 °C)	
3.6×10^3 s	13.50
2.16×10^4 s	13.20
8.64×10^4 s	13.20

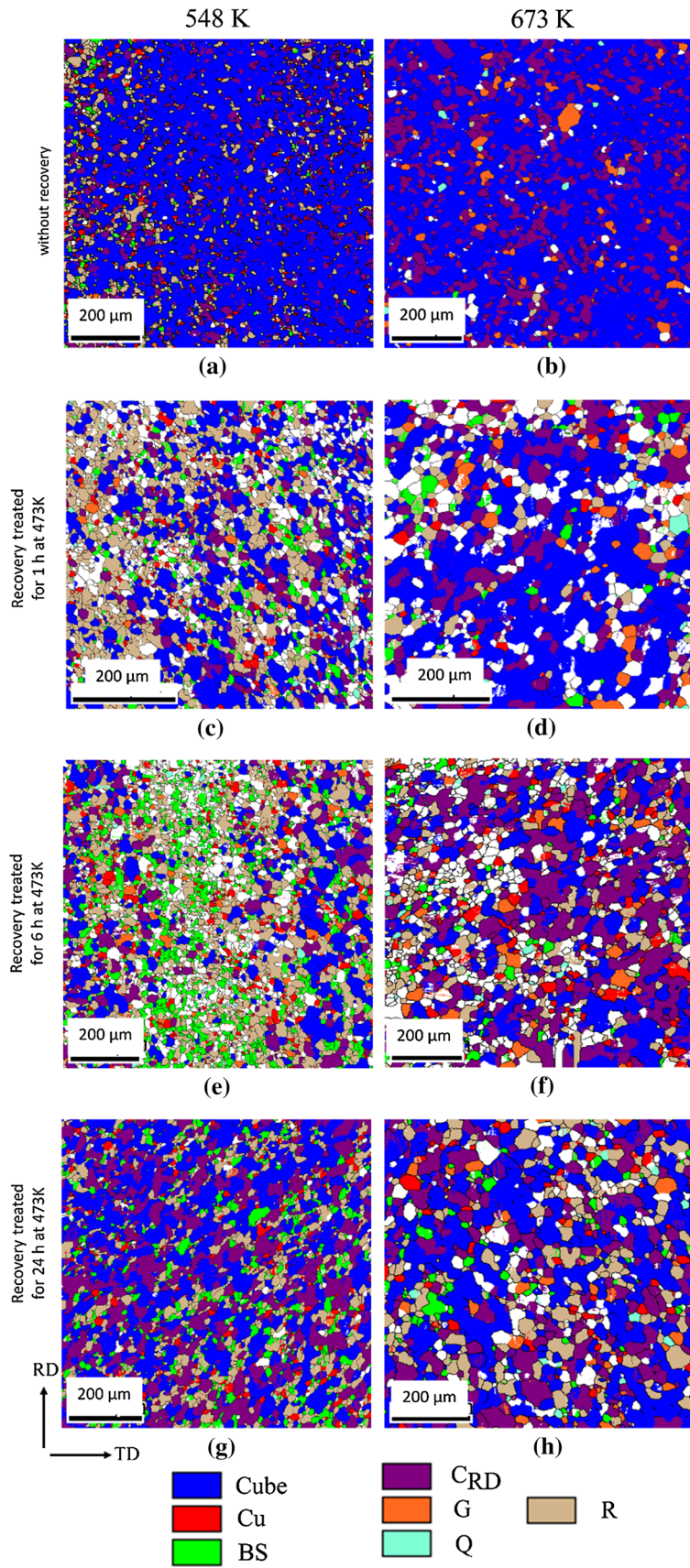


Fig. 5—Orientation maps of warm-rolled sheets annealed (*a, b*) without and (*c* through *h*) with different prior recovery treatments.

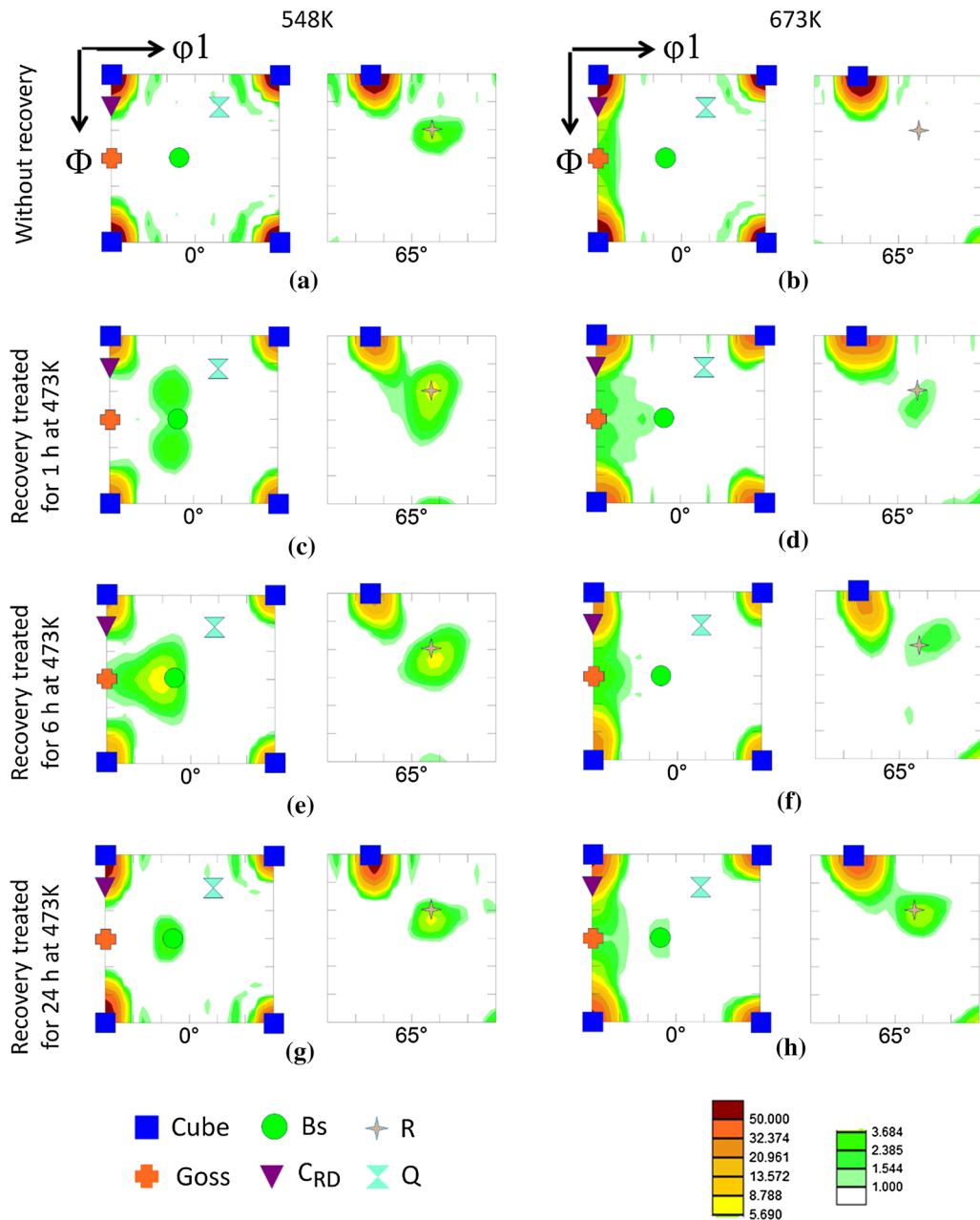


Fig. 6—Relevant ODF sections of warm-rolled sheets annealed (*a, b*) without and (*c* through *h*) with different prior recovery treatments.

Table III shows the variation in the average cube and non-cube grain size in materials annealed at 548 K and 673 K (275 °C and 400 °C) with and without prior recovery treatments. The average grain size of the cube is evidently higher than the average size of the non-cube grains (>15 deg misorientation with the exact cube location).

IV. DISCUSSION

The most important observation in the present work is that different pre-recovery treatments greatly reduce the strength of the cube texture of severely warm-rolled Al-2.5 pctMg alloy after annealing. In the light of the

two contrasting theories of the formation of recrystallization texture already introduced, it may be interesting to reveal the relative importance of nucleation and growth of cube grains in order to explain the effect of prior recovery treatments on the formation of cube texture.

In order to understand the mechanism of formation of cube texture, the warm-rolled material without any pre-recovery treatment is annealed at 523 K (250 °C) for 300 seconds. The material which has been pre-recovered at 200 °C (473 K) for 3.6×10^3 seconds (1 hour) is annealed at 523 K (250 °C) for 3.6×10^3 seconds (1 hour). As will be shown, these heat treatments result in similar average recrystallized volume fraction in the two materials.

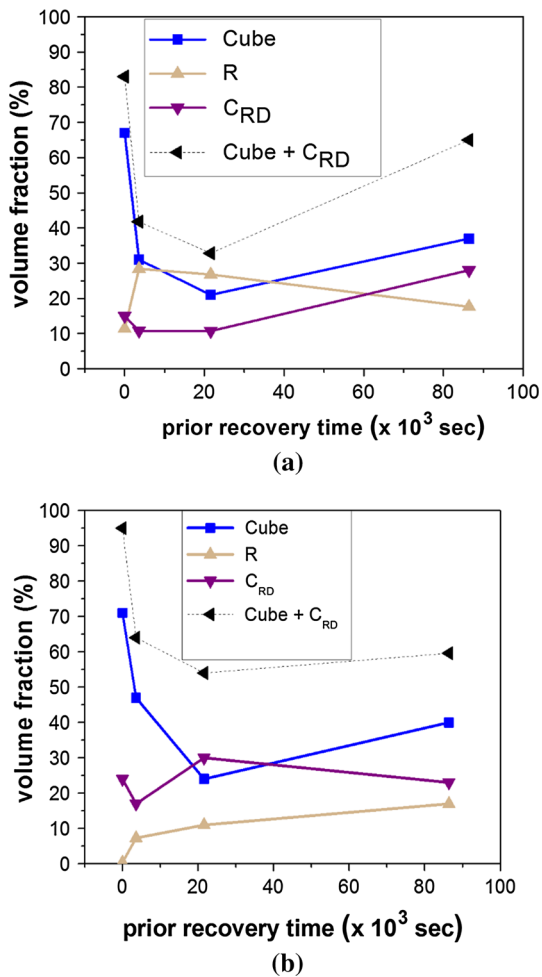


Fig. 7—Variation in the volume fractions of important texture components during annealing of 97 pct warm-rolled Al-2.5 wt pctMg alloy at (a) 548 K (275 °C) and (b) 673 K (400 °C) without (corresponding to zero prior recovery time as shown in the plot) and with prior recovery treatment.

The internal misorientation distribution maps (kernel average misorientation or KAM) of the partially recrystallized materials without any pre-recovery treatment (Figure 8(a)) reveal early recrystallized grains surrounded by deformed regions. The deformed regions are clearly distinguished from the recrystallized grains by higher KAM and the presence of LAGB network. It is thus clearly understood that the recrystallized regions should have lower internal misorientation as compared to the deformed regions. Accordingly, the recrystallized regions are defined as those regions having KAM ≤ 1 deg and grain size (area) $\geq 4 \mu\text{m}^2$. The KAM values are determined up to three nearest neighbors using a maximum tolerance of 5 deg. Similar criteria have been used by other authors to isolate recrystallized regions in partially recrystallized materials^[37,38] which yield quite satisfactory results. In addition, it is further confirmed that the recrystallized grains are separated from the surrounding matrix by HAGBs over large parts of their circumference. The average recrystallized volume fraction is found to be similar ~ 10 pct. The orientation map of the recrystallized regions (the deformed regions are

masked) is shown in Figure 8(b). The orientation map shows (Figure 8(b)) profuse cube-oriented grains. The orientation data of more than 500 early recrystallized grains obtained from different regions of the partially recrystallized material are examined which reveal that the number fraction of cube-oriented grains is ~ 0.30 . Figure 8(c) shows the $\varphi_2 = 0$ deg section of the ODF calculated from the recrystallized fraction using the average orientation of each individual grain but disregarding the area of the grains. The ODFs calculated in this manner are thus affected only by the frequency of each orientation. Strong intensities could be easily be observed at the vicinity of the cube orientation, which clearly indicates the strong presence of cube orientation at an early stage of recrystallization or strong preference for ON of cube grains.

The KAM distribution map of the pre-recovery-treated material in the partially recrystallized condition (Figure 8(d)) also reveals clear recrystallized grains surrounded by deformed regions. Applying the same set of criteria, the recrystallized regions are separated from the deformed regions. The average recrystallized volume fraction is ~ 12 pct, which is similar to the material which is partially recrystallized without any pre-treatment (Figure 8(a)). In sharp contrast to the material without pre-recovery treatment (Figure 8(b)), the orientation map of the recrystallized fraction in the pre-recovery-treated specimen shows the presence of very few cube-oriented grains (Figure 8(e)). The average number fraction of cube-oriented grains is only ~ 0.1 which is much lower than the number fraction of cube grains in the partially recrystallized material without any pre-recovery treatment (Figure 8(b)). The ODF is calculated from the recrystallized fraction considering the average orientation of each recrystallized grain. The $\varphi_2 = 0$ deg section (Figure 8(f)) of the ODF shows the presence of weak cube texture in the recovery-treated material as compared to the material without pre-recovery at early stages of recrystallization. This clearly indicates diminished preference for ON of cube grains in the prior recovery-treated material. Thus, the significantly weakened cube texture in different pre-recovery-treated materials as compared to the material without any prior recovery treatment could be convincingly attributed to the starkly different nucleation behavior of cube grains in the two cases. It may be noted that prior recovery treatment has also been reported to be detrimental to the development of the cube texture.^[26,27] However, as compared to the cold-rolled Al-Mg alloy,^[26] the weakening of the cube texture due to prior recovery treatments is much stronger in warm-rolled alloys.

The preferential nucleation of cube grains in the ON model is explained by the lower stored energy or more recovered structure of cube regions in deformed matrix resulting from the interaction of dislocation with orthogonal burgers vectors.^[21] The more recovered structure of the cube regions ensures localized differences in the stored energy^[39] resulting in preferential nucleation of cube grains. However, in Al-Mg alloys, the dislocations are strongly pinned by Mg atoms due to which dynamic recovery is strongly inhibited during

deformation at ambient temperatures.^[22] As a result, the strength of the cube texture in cold-rolled and annealed Al-Mg alloys is rather weak. However, during warm-rolling at elevated temperature, the pinning force will be reduced. Since the holding time at the warm-rolling temperature is short, the cube regions may undergo preferential dynamic recovery due to their tendency for accumulating lower stored energy. In other words, the warm-rolled material exhibits strong orientation dependent recovery. This results in the preferential nucleation of cube grains (*i.e.*, strong ON behavior) leading to the formation of strong cube texture in warm-rolled and annealed Al-Mg alloy.

As already explained, due to the strong pinning effect of Mg atoms, both dynamic and static recovery will be significantly inhibited in Al-Mg alloys. As a result, stored energy of warm-rolled Al-Mg will be rather high, which in turn will provide high driving force for recovery during the prior recovery treatment. In Al-Mg

alloy, these conflicting factors exert a net effect on the recovery behavior, such that the recovery in cold-rolled Al-Mg alloy can be surprisingly fast.^[22,40,41] The homogenous recovery process during different prior recovery treatments is amply supported by the microstructural (Figure 3), textural (Figure 4), and conductivity measurements (Table III). Homogenous recovery results in reduced driving force for recrystallization so that in order to obtain a similar recrystallized volume fraction, the pre-recovery-treated sample has to be annealed for a longer time (1 hour) as compared to the material without any prior recovery treatment (300 seconds) (Figure 8). The diminished tendency for the preferential nucleation of cube grains in the pre-recovery-treated material can be convincingly attributed to the homogenous recovery process during the pre-recovery treatment. Homogenous recovery in Al-Mg alloy greatly reduces the stored energy difference of the cube and surrounding regions. This effectively diminishes the

Table III. Variation in Cube and Non-cube Grain Size in Annealed Materials Without and with Different Prior Recovery Treatments

Recovery Time at 473 K (200 °C)	Annealing Temperature			
	548 K (275 °C)		673 K (400 °C)	
	Cube (μm)	Non-cube (μm)	Cube (μm)	Non-cube (μm)
0 s (without recovery)	15	10	18	15
3.6×10^3 s (1 h)	12	8	18	14
2.16×10^4 s (6 h)	18	11	21	17
8.64×10^4 s (24 h)	18	10	19	16

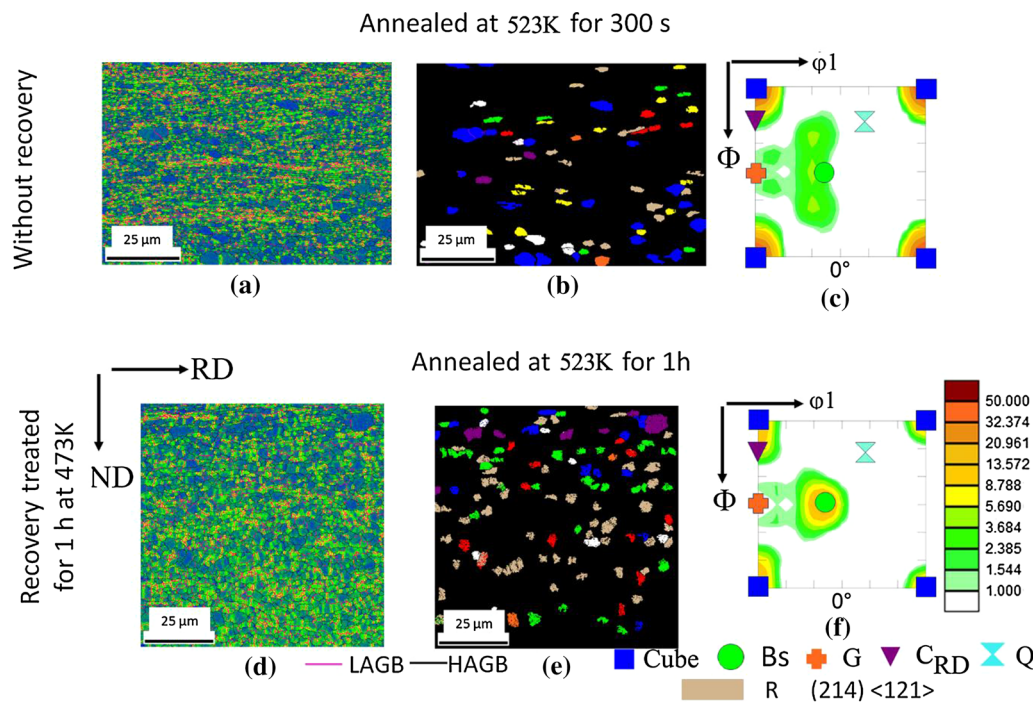


Fig. 8—(a, d) KAM maps, (b, e) orientation maps of recrystallized regions, and (c, f) $\phi_2 = 0$ deg section of the ODFs of warm-rolled material without (a through c) and (d through f) with prior recovery treatments after annealing at 523 K (250 °C) for 300 s and 3.6×10^3 s (1 h), respectively.

nucleation advantage of cube regions originating from their preferentially recovered structure. This evidently leads to significant weakening of the cube texture after annealing in different pre-recovery-treated materials.

The average size of the cube grains is found to be much larger than the average size of the non-cube grains in different materials (Table III). This indicates a preferential growth behavior of cube grains. However, the strength of the cube texture after annealing is starkly different in materials without and with different pre-recovery treatments which further proves that ON behavior of cube grains determines the strength of the cube texture upon annealing. It must be pointed out that while a general preferential growth behavior of cube grains can be understood; however, this also involves significant post-recrystallization grain growth at the two annealing temperatures. The strengthening of the cube texture during grain growth is explained on the basis of the total reduction of grain boundary energy. Stronger cube texture can result in a microstructure dominated by $\Sigma 1$ or LAGB network, reducing the total energy of the grain boundaries.^[42] However, with regard to the prior recovery time, some differences could still be observed. Particularly for the material prior recovery treated for 6 hours, the cube volume is lower after different annealing treatments as compared to those in the materials prior recovery treated for 1 and 24 hours. The orientation maps (Figure 5) and analysis in Figure 7 clearly indicate that these differences originate from the relative strength of the C_{RD} component. It may be presumed that microtexture differences can result in such differences.

In summary, prior recovery treatment greatly diminishes the strength of the cube texture in severely warm-rolled and annealed Al-Mg alloy. It is quite apparent that introducing suitable prior recovery treatments in the thermo-mechanical processing cycle can be a novel way for controlling cube texture and tailoring the anisotropic mechanical behavior.

V. CONCLUSIONS

From the present study, the following conclusions may be drawn:

- Development of lamellar deformation structure and strong pure metal type texture could be observed after severe warm rolling of Al-2.5 wt pctMg alloy.
- The warm-rolled material without any pre-recovery treatment develops strong cube texture after annealing. However, different pre-recovery treatments greatly diminish the strength of the cube texture upon annealing.
- The formation of strong cube texture in warm-rolled materials without any pre-recovery treatment is attributed to the preferential nucleation of cube grains.
- Prior recovery treatments lead to homogenous recovery, which greatly diminish the nucleation advantage of cube grains in terms of their preferentially recovered structure. This results in a dimin-

ished tendency for the preferential nucleation of cube grains and leads to the weakening of the cube texture upon annealing.

- The cube texture is strengthened with increasing annealing temperature due to the growth of the cube grains.
- The present results indicate that prior recovery treatment can be effectively used to control recrystallization cube texture in severely warm-rolled aluminum alloys.

ACKNOWLEDGMENT

The authors acknowledge the financial support of DST, India through Grant No. SR/FTP/ETA-126/2010.

REFERENCES

1. J. Hirsch and K. Lucke: *Acta Metall.*, 1988, vol. 36, pp. 2863–82.
2. J. Hirsch, K. Lucke, and M. Hatherly: *Acta Metall.*, 1988, vol. 36, pp. 2905–27.
3. T. Leffers and R.K. Ray: *Prog. Mater. Sci.*, 2009, vol. 54, pp. 351–96.
4. O. Engler: *Scripta Mater.*, 2001, vol. 44, pp. 229–36.
5. O.V. Mishin, A. Godfrey, D. Juul Jensen, and N. Hansen: *Acta Mater.*, 2013, vol. 61, pp. 5354–64.
6. O. Engler, H.E. Vatne, and E. Nes: *Mater. Sci. Eng. A*, 1996, vol. 205, pp. 187–98.
7. O. Engler: *Metall. Mater. Trans. A*, 1999, vol. 30A, pp. 1517–27.
8. W.C. Liu and J.G. Morris: *Mater. Sci. Eng. A*, 2003, vol. 363, pp. 253–62.
9. W.C. Liu, T. Zhai, C.S. Man, and J.G. Morris: *Scripta Mater.*, 2003, vol. 49, pp. 539–45.
10. K. Lucke and O. Engler: *Mater. Sci. Tech.*, 1990, vol. 6, pp. 1113–30.
11. O. Daaland and E. Nes: *Acta Mater.*, 1996, vol. 44, pp. 1413–35.
12. W.C. Liu and J.G. Morris: *Metall. Mater. Trans. A.*, 2005, vol. 36A, pp. 2829–48.
13. C. Schäfer and G. Gottstein: *Int. J. Mater. Res.*, 2011, vol. 102, pp. 1106–14.
14. K. Huang, O. Engler, Y.J. Li, and K. Marthinsen: *Mater. Sci. Eng., A*, 2015, vol. 628, pp. 216–29.
15. R.D. Doherty, D.A. Hughes, F.J. Humphreys, J.J. Jonas, D. Juul Jensen, M.E. Kassner, W.E. King, T.R. McNelley, H.J. McQueen, and A.D. Rollett: *Mater. Sci. Eng. A*, 1997, vol. 238, pp. 219–74.
16. I.L. Dillamore and H. Katoh: *Met. Sci. J.*, 1974, vol. 8, pp. 73–83.
17. I. Samajdar and R.D. Doherty: *Acta Mater.*, 1998, vol. 46, pp. 3145–58.
18. H.E. Vatne, T. Furu, R. Ørsund, and E. Nes: *Acta Mater.*, 1996, vol. 44, pp. 4463–73.
19. J.C. Glez and J.H. Driver: *Acta Mater.*, 2003, vol. 51, pp. 2989–3003.
20. G. Guiglionda, A. Borbély, and J.H. Driver: *Acta Mater.*, 2004, vol. 52, pp. 3413–23.
21. A.A. Ridha and W.B. Hutchinson: *Acta Metall.*, 1982, vol. 30, pp. 1929–39.
22. F.J. Humphreys and M. Hatherly: *Recrystallization and Related Annealing Phenomena*, 2nd ed., Elsevier, Oxford, 2004.
23. K. Huang, N. Wang, Y. Li, and K. Marthinsen: *Mater. Sci. Eng. A*, 2014, vol. 601, pp. 86–96.
24. M.H. Alvi, S.W. Cheong, J.P. Suni, H. Weiland, and A.D. Rollett: *Acta Mater.*, 2008, vol. 56, pp. 3098–108.
25. M.Y. Huh, S.Y. Cho, and O. Engler: *Mater. Sci. Eng., A*, 2001, vol. 315, pp. 35–46.
26. W.C. Liu, J. Li, H. Yuan, and Q.X. Yang: *Scripta Mater.*, 2007, vol. 57, pp. 833–36.

27. K. Huang, Y.J. Li, and K. Marthinsen: *Mater. Charact.*, 2015, vol. 102, pp. 92–97.
28. H. Inoue and T. Takasugi: *Mater. Trans.*, 2007, vol. 48, pp. 2014–22.
29. O. Engler, H.C. Kim, and M.Y. Huh: *Mater. Sci. Tech.*, 2001, vol. 17, pp. 75–86.
30. J.R. Gatti and P.P. Bhattacharjee: *J. Alloy. Compd.*, 2014, vol. 615, pp. 950–61.
31. M.Y. Huh, H.D. Kim, K.R. Lee, B.B. Hwang, and O. Engler: *Mater. Sci. Forum*, 2002, vols. 408–412, pp. 1453–58.
32. N. Tsuji, Y. Saito, S.H. Lee, and Y. Minamino: *Adv. Eng. Mater.*, 2003, vol. 5, pp. 338–44.
33. T. Yu, N. Hansen, and X. Huang: *Acta Mater.*, 2013, vol. 61, pp. 6577–86.
34. T. Yu, N. Hansen, and X. Huang: *Proc. R. Soc. Lond. A Mat.*, 2011, vol. 467, pp. 3039–65.
35. L. Radovic and M. Nikacevic: *Sci. Tech. Rev.*, 2008, vol. 58, pp. 14–19.
36. H. Takuda, N. Yamazaki, N. Hatta, and S. Kikuchi: *J. Mater. Sci.*, 1995, vol. 30, pp. 957–63.
37. X.L. Li, W. Liu, A. Godfrey, D. Juul Jensen, and Q. Liu: *Acta Mater.*, 2007, vol. 55, pp. 3531–40.
38. P.P. Bhattacharjee, R.K. Ray, and N. Tsuji: *Acta Mater.*, 2009, vol. 57, pp. 2166–79.
39. S. Raveendra, S. Mishra, K.V.M. Krishna, H. Weiland, and I. Samajdar: *Metall. Mater. Trans. A*, 2008, vol. 39A, pp. 2760–71.
40. C. Bairoz, 3rd International Conference on Aluminum Alloys (ICAA 3), Trondheim, Norway, 22–26 June, 1992.
41. E.C.W. Perryman: *Trans. Am. Inst. Min. Metall. Eng.*, 1955, vol. 203, pp. 369–78.
42. N.M. Hwang: *Scripta Mater.*, 1997, vol. 37, pp. 1637–42.